Investigating the effect of tungsten initial microstructure on restoration kinetics using a mean field model

Maxime Lemetais, Alan Durif, David Piot, Matthieu Lenci, Marianne Richou, Guillaume Kermouche

Investigating the effect of tungsten initial microstructure on restoration kinetics using a mean field model

Maxime LEMETAIS[a,b,c], Alan DURIF[b], David PIOT[a], Matthieu LENCI[a], Marianne RICHOU[b], Guillaume KERMOUCHE[a]

(a) Mines Saint-Etienne, CNRS UMR 5307 LGF, Centre SMS, F – 42023 ST ETIENNE CEDEX, France
(b) CEA, IRFM, F – 13108 ST PAUL LEZ DURANCE CEDEX, France
(c) Aix-Marseille Univ, CNRS, Centrale Marseille, Institut Fresnel, 13000 MARSEILLE, France

Keywords:

Mean-field model, recrystallization, recovery, tungsten, softening, thermonuclear fusion

Abstract:

Tungsten is the privileged option as plasma-facing material for the divertor region of ITER and DEMO tokamaks. Under repeated high thermal fluxes (10 MW/m² in steady state and 20 MW/m² in quasi-steady state), Plasma-Facing Units (PFU) can be damaged through thermal fatigue phenomena, which are enhanced by in-service tungsten recrystallization. Slowing down tungsten recrystallization is thus a way to optimize PFU lifetime. Tungsten-recrystallization kinetics is known to depend upon the initial microstructure. In the present paper, a mean-field model [1] is developed to highlight microstructural effects upon tungsten restoration mechanisms at high temperature. The effects of grain size, initial recrystallized fraction, initial dislocation density, i.e stored energy, and dislocation density distribution have been investigated. It is clearly quantified how a higher stored energy can lead to a drastic increase of the recrystallization rate. It is also shown how a prior recovery stage helps to slow down recrystallization. Finally, a conclusion is brought upon the ability of such a mean field model to optimize the tungsten initial microstructure for fusion engineering.

Introduction

In nuclear fusion machine, plasma-facing materials (PFM) constitute the first inner wall facing the plasma. In ITER, tungsten as PFM will have to endure high thermal fluxes in the divertor region going from 10 MW/m² in steady state to 20 MW/m² in quasi-steady state [2]. Thermomechanical simulations and experimental studies reveal that cracks could appear in tungsten PFM in the divertor region during ITER operations [3–4]. Cracking probability highly depends on the mechanical properties of tungsten [5]. Both recrystallization and recovery are thermally-activated restoration mechanisms [5–7], that lead to tungsten softening [6] and are known to be both detrimental to thermal fatigue resistance. Recrystallization is based on the nucleation of new grains which grow at the expense of the former-deformed tungsten grains. Recovery is characterized by the decrease of dislocation density within the grains. In both cases, the driving force is related to the stored energy, i.e. the dislocation density.

Empirical model like Johnson-Mehl-Avrami-Kohlmogorov (JMAK) can assess softening kinetics [7]–[9]. Within JMAK framework, nucleation rate and grain growth are supposed to be constant. Recrystallization and recovery mechanisms are usually disconnected [7]. JMAK model has been used in previous studies to assess recrystallization kinetics of tungsten [10]–[16]. JMAK kinetics give a relevant description of the mechanical property evolution, as hardness during isothermal annealings, but does not permit to assess the softening evolution according to the initial microstructure of tungsten, or plasma facing conditions such as anisothermal loading coupled with irradiation or plasma exposure. By contrast, full-field models, based on the full microstructure description, are able to assess the evolution of a given microstructure with high accuracy but are expansive in terms of experimental characterizations and computation time [17]. Mean-field models have also been used to study tungsten softening kinetics[1], [18]. Those models cost less than full-field models and can account for microstructural properties of tungsten in softening predictions[18], [19]. In the present article, the mean-field model described by Durif et al. [1] is used to assess the impact of different initial microstructures on softening and recrystallization kinetics. Model parameters are based on the analysis of high-temperature annealing experiments [12] and have been extracted from Durif et al. [1]. Mean-field model allows to assess the features of the initial microstructure responsible for the loss of mechanical properties that could be detrimental for ITER and future nuclear fusion power plants using tungsten as plasma facing materials [5], [20], [21]. In this article, the mean-field model developed was used to quantify the impact of grain size, initial recrystallized fraction, and dislocation density on the restauration kinetics at different temperature. The mean-field model developed by A. Durif, [1] is able to take into account recovery and grain growth related to the difference of energy stored in dislocations between deformed and recrystallized grains during post-dynamic recrystallization where deformed grains are still largely present in the microstructure. This model do not take into account grain growth mechanism related to the texture of the microstructure, topological effects or the impact of grain size on grain boundary migration.

The mean-field model developed [1] have already been used on two different tungsten materials coming from two different suppliers. After fitting a common recovery and grain boundary mobility parameters for both materials, the model correctly predicted softening and recrystallization fraction during annealing at different temperature between 1400°C and 1800°C [1].

The first section presents the equations governing the mean field model. The impact of various microstructural parameters on the simulated recrystallization kinetics are then investigated. A specific attention is brought to microstructural parameters related to the

stored energy, such as the initial dislocation density or the initial fraction recrystallized. Finally, the article concludes on the ability of such a model to guide the design of tungsten microstructures for fusion engineering.

I. Mean-field model structure and parameters

The mean-field model developed by Durif [1] can be split into three steps. In a first step, material properties, annealing conditions and computational parameters are addressed. In a second step, annealing is simulated and results are extracted in the last part. Annealing is discretized in time increments. At each increment, microstructural parameters such as grain radii R_i and dislocation densities ρ_i are modified according to two equations [1] describing (i) grain boundary migration (Equation 1) in which $\overline{\rho(t)}$ is for the mean dislocation density, M is the grain-boundary mobility, and (ii) recovery (Equation 2) in which r is the parameter of recovery kinetics. In a mean-field model, a homogeneous equivalent medium (HEM) describes surroundings of the grain [17], [22], [23]. The parameters of the HEM corresponds of the mean properties of the microstructure. The grain radii $\boldsymbol{R_i}$ evolve according to the difference between the average dislocation density of the HEM $\overline{\boldsymbol{\rho(t)}}$ and the dislocation density of a given grain *i*. All the parameters are assumed to depend only on temperature and have been fitted to recrystallized and softening fractions obtained by EBSD and hardness measurements on two different materials at four annealing temperatures [1,12]. The Durif et al. model assumes that the recovery of each grain does not depend on the HEM parameters. After applying radius and dislocation-density evolutions for each grain, HEM parameters, *i.e*. mean dislocation density $\overline{\boldsymbol{\rho(t)}}$ computed from the resulting microstructure are actualized according to $\overline{\rho(t)} = \frac{\sum_{i=1}^{n} \rho_i(t) {R_i}^2(t)}{\sum_{i=1}^{n} {R_i}^2(t)}$ (Equation 5). Macro-parameters (i.e. recrystallized and softening fractions) are updated at each time step. Recrystallized fraction *X* (Equation 3) equals to the sum of the volume of each recrystallized grain on the sum of the volume of all grains. Softening fraction *Xh* (Equation 4) corresponds to the average flow stress per volume unit of each grain added to the hardness $\boldsymbol{H_{recr}}$ (Equation 5) of the recrystallized material [1]. The hardness of the initial deformed material without any recrystallized grains $\boldsymbol{H_{def}}$ is assessed from the initial hardness $\boldsymbol{H_0}$, the hardness of the recrystallized material $\boldsymbol{H_{recr}}$ and the initial recrystallized fraction $\boldsymbol{X_{init}}$ (Equation 6) [1].

$$\dot{R}_i = M\tau\left(\overline{\rho(t)} - \rho_i(t)\right)$$

Equation 1

$$\rho_i(t) = \rho_{0,i} e^{-rt}$$

Equation 2

$$X = \frac{\sum_{i=1}^{n} {R_{i,recr}}^3(t)}{\sum_{i=1}^{n} {R_i}^3(t)}$$

Equation 3

$$Xh = \frac{H_{def} - H_v(t)}{H_{def} - H_{recr}}$$

Equation 4

$$H_v(t) = H_{recr} + 3G_{20°C} b \frac{\sum_{i=1}^{n} {R_i}^3(t)\sqrt{\rho_i(t)}}{\sum_{i=1}^{n} {R_i}^3(t)}$$

Equation 5

$$H_{def} = \frac{H_0 - X_{init} H_{recr}}{1 - X_{init}}$$

Equation 6

For each time step, the operations listed above are repeated. Recrystallization phenomenon occurring after dynamic recrystallization is usually called post-dynamic recrystallization. At the end of hot-rolling process, nuclei without dislocations can already be present in the microstructure [24], [25]. Material that have been studied in Durif et al. have been hot-rolled and probably submitted to an undocumented annealing [1], [12]. EBSD data treatment on initial sample before laser annealing already reveals nuclei on these material [1], [12]. Hardness is computed at 20 °C because hardness measurement performed to calibrate the model where done at around 20 °C [12]. The shear modulus $G_{20°C}$ of tungsten under consideration is therefore taken at 20 °C for the assessment of hardness. The Burgers vector b is $2.73.10^{-10}$ m.

Mobility and recovery parameters are fitted on the recrystallized and softened fractions estimated by EBSD and hardness on two tungsten materials studied by Richou [12]. Mobility and recovery used for each temperature are reported in **Erreur ! Source du renvoi introuvable.**.

Temperature (°C)	Recovery (s^{-1})	Mobility ($m.Pa^{-1}.s^{-1}$)

1450	2.97e−4	1.91e−15
1500	8.48e−4	7.37e−15
1550	1.47e−3	3.56e−14
1600	4.76e−3	1.735e−13

Table 1. Recovery and mobility parameter used for the computation of the mean field model used in Equation 1 and Equation 2

The hardness of recrystallized tungsten is assumed 359 HV in all simulations. The influence of time step is found to be negligible under 10 seconds except for annealing at 1600 °C. Time step is chosen to be 10 seconds for all temperatures excepted 1600 °C. For the simulation of the annealing at 1600 °C the time step has been reduced to 1 s. In Durif [1], grain sizes are fitted by a log-lognormal distribution and distribution tail are truncated. Log-lognormal distribution and truncation of the tail have been also used. The maximum radius is 42 µm for deformed grains and 7.6 µm for recrystallized grains according to Durif et al. [1]. The impact of the distribution of initial dislocation density has been assessed while applying constants for the initial radius of deformed and recrystallized grains. The influence of initial fraction recrystallized, initial dislocation density in the deformed grains and the radius distribution of recrystallized and deformed grains have been investigated by applying small variations from the tungsten material studied in Durif et al. [1] (grade A).

II. Results and discussions

a. Impact of initial recrystallized fraction (initial X)

In the mean field model developed by Durif et al. [1], nucleation is supposed to have already happened [12]. This assumption is based on the initial recrystallized fraction estimated from EBSD data treatment to be 15 % for the first material studied called grade A and 7 % for the material called grade B [12]. In order to be consistent with this assumption, the lowest initial recrystallized fraction studied was 5 % and the highest initial recrystallized fraction studied was set to 25 %. In a material with an initial recrystallized fraction of 25 %, it is assumed that dislocation density in the deformed grains is still high enough to well describe softening process in the first 4000 s of annealing. Dislocation density in the deformed grains was supposed to be uniform and equals to $4.81.10^{13}$ m^{-2} at the initial state. Recrystallized and deformed grain-radius distribution parameters are the same between each simulations. Therefore, the number of initial recrystallized grains is higher when the initial recrystallized fraction has been increased. Dislocation density is identical between each simulations. The initial hardness is higher when the initial recrystallized fraction is higher. Initial hardness varies between 426 HV and 444 HV. These are consistent with those find in literature [10]–[12].

According to the simulations, for a higher initial recrystallized fraction, softening fraction is greater at a given time and temperature (Figure 1a, Table 2). With this set of parameters, recrystallization only plays a role at the beginning of the annealing while the dislocation density in the deformed grains is still high (Figure 1b, Table 2). At the end of annealing, only recovery plays a role. Half-softening time corresponds to the annealing duration required for the tungsten to loose half of its hardness. Half-softening time is reached earlier at higher temperature (Figure 1c, Table 2). Initial recrystallized fraction also lowers the time required to reach half-softening time. However, simulations reveals no apparent coupling between the effect of initial recrystallized fraction and temperature to reach half-softening time. Dislocation density in deformed grains reach a value of $6.7.10^{10}$ m^{-2} after 10 000 s at 1500 °C in each simulation. After 4000 s, no more recrystallization occurs. For each simulation, the difference between initial and final recrystallized fraction is comprised between 15 to 17 % at 1500 °C. This is consistent with the model because according to Equation 3 recrystallization driving force is only based on dislocation density between HEM and each grain. Dislocation density in the HEM is lower for a higher recrystallized fraction while initial dislocation density remains the same for each simulation. This implies that recrystallization driving-force would be higher for lower recrystallized fraction. The relative contribution of recrystallization to softening increases with temperature.

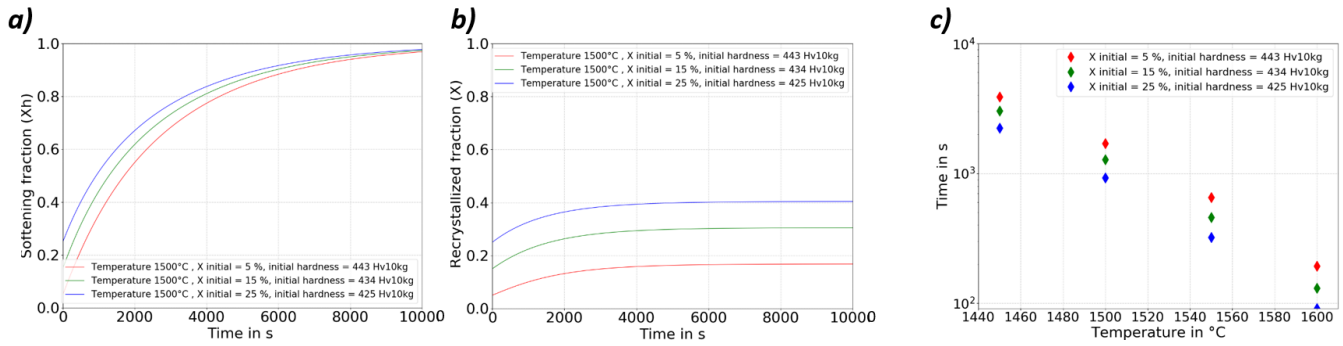

Figure 1a) Softening kinetics at 1500 °C for different initial recrystallized fraction. b) Recrystallization kinetics at 1500 °C for different initial recrystallized fraction. c) Half-softening time as a function of temperature for different initial recrystallized fraction.

b. Influence of initial dislocation density (ρ_{def})

Initial dislocation density is supposed to be identical in each deformed grain in the present section. Initial dislocation density is assessed from hardness and EBSD according to Tabor law and Taylor relation in Durif (Equation 7).

$$\rho_{def,init} = \left(\frac{HV_{\text{init}} - HV_{\text{recr}}}{3(1 - X_{\text{init}}) G_{20°C} b_g} \right)^2$$

Equation 7

Supposing a recrystallized fraction of 15 % and a hardness of 359 HV for all the recrystallized grain, the initial hardness of the tungsten material varies between 402 HV and 490 HV for a mean initial dislocation density varying between $1.6.10^{13}$ m^{-2} and $1.44.10^{14}$ m^{-2} in the deformed grains (Table 3). The initial hardness listed in Table 3 has been chosen in regards to the one of deformed tungsten [10]–[12], [26], [27]. The dislocation densities mentioned in Table 3 are those of deformed grains, the dislocation density in recrystallized grains being set to zero. It is assumed that an increase of the initial dislocation density does not involve a second nucleation that could have significant impact during annealing. If second nucleation happened for this kind of material, softening kinetics maybe accelerated even further for higher dislocation density. At the beginning of annealing simulation, recrystallization have a much more important impact on softening for higher initial dislocation density (Figure 2a and Figure 2b, and Table 3). The evolution of half-softening time (Figure 2c, Table 3) illustrates the impact of competition between recovery and recrystallization for different dislocation density at 5 various temperatures. The impact of dislocation density on softening fraction is enhanced at higher temperature. Hardness is greater for materials with higher initial dislocation density after 4000 s at 1500 °C. However, at 1550 °C for a material with a higher initial dislocation density, the hardness is lower after 4000 s. The relative impact of recrystallization compared to recovery increases when initial dislocation density or temperature is increased.

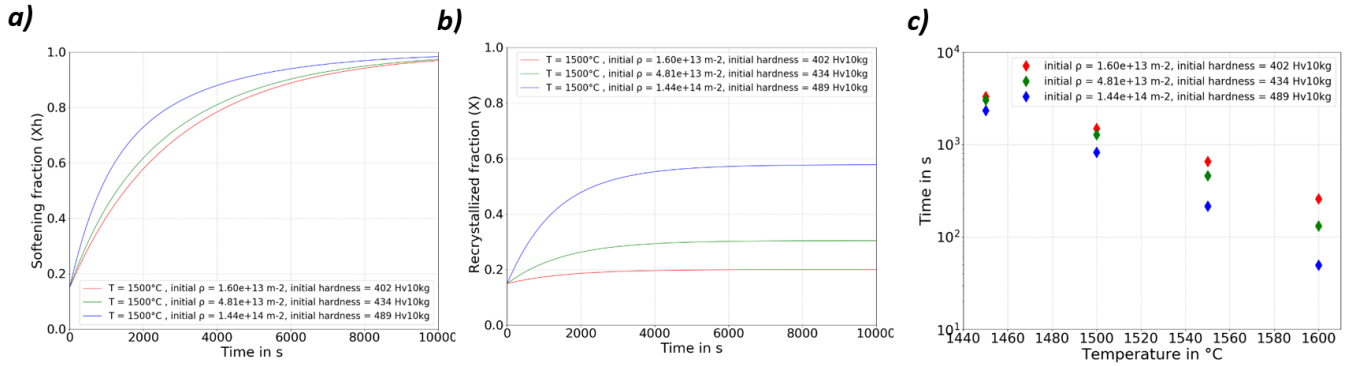

Figure 2a) Softening kinetics at 1500 °C for different initial dislocation densities in deformed grain. b) Recrystallization kinetics at 1500 °C for different initial dislocation densities in deformed grains. c) Half-softening time as a function of temperature for different initial dislocation densities.

c. Role of recrystallized and deformed grain distributions

Initial radius distributions for deformed and recrystallized grains are assumed to be log-lognormal in Durif [1]. This assumption appears still valid and distribution parameters are slightly changed in order to get broader or thinner distributions. It is shown to not impact much the evolution of the recrystallized and softening fraction simulated by mean-field model (Figure 3 and Table 4). A slight variation of the radius distributions of deformed grains has almost no impact on recrystallization softening kinetics (Table 4, Figure 3).

$$cdf(R) = 1/2 \left[1 + \text{erf} \left[\frac{\ln(\ln(R)) - \mu}{\sigma\sqrt{2}} \right] \right]$$

Equation 8

The cumulative density function for a log-log normal distribution is given in Equation 8 where *R* stands for the radius in µm. The parameters used to estimate the initial radius of deformed grains are summarized in Table 4, µ and σ being the parameters of the log-normal distributions.

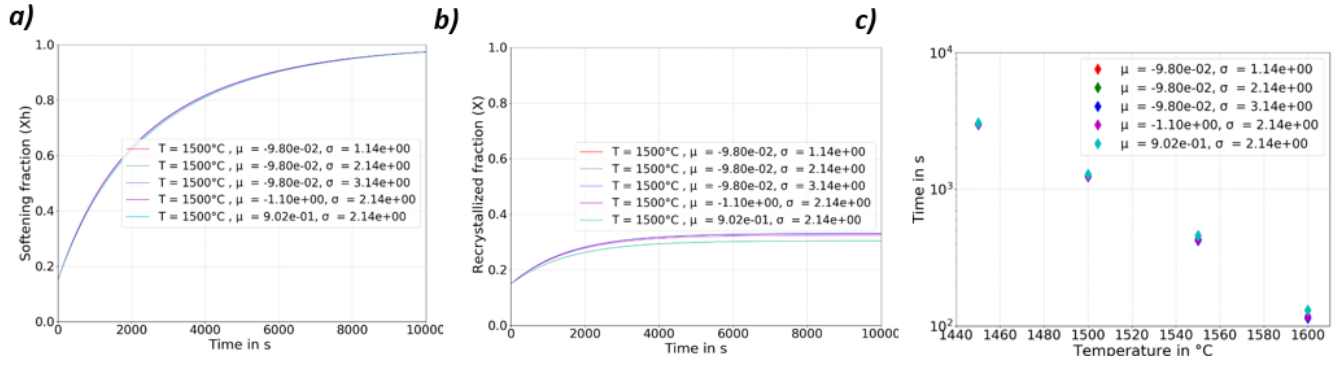

Figure 3a) Softening kinetics at 1500°C for different initial deformed grain radius distributions. b) Recrystallization kinetics at 1500°C for different initial deformed grain radius distribution. c) Half-softening time as a function of temperature for different initial deformed grain radius distributions.

d. Influence of dislocation density distribution

The distribution, among the deformed grains, of dislocation density is now considered (instead of using a constant value). The mean value of each dislocation density distribution is around 4.81e13 m^{-2} (Table 5). The different distributions have only broader or thinner aspects. It is found that the aspects of those distributions does not influence softening kinetics during annealing (Figure 4). Two constants are used for the radii of deformed and recrystallized grains instead of using log-lognormal distributions. A slight variation of dislocation density distribution does not impact softening kinetics. However, recrystallization kinetics are modified (Figure 1, Table 5).

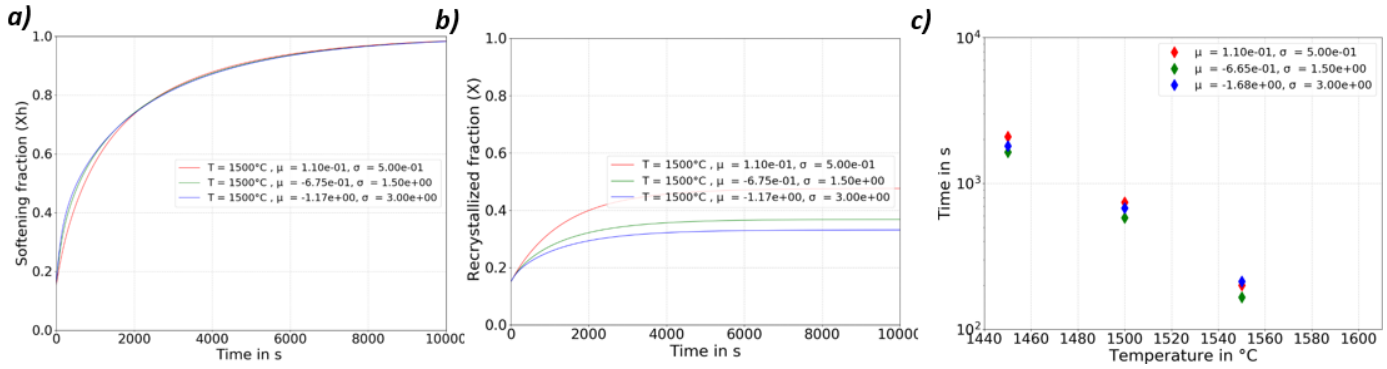

Figure 4a) Softening kinetics at 1500 °C for different initial dislocation density distributions. b) Recrystallization kinetics at 1500 °C for different initial dislocation density distributions. c) Half-softening time as a function of temperature for different initial dislocation density distributions.

Conclusions

A parametric study of the mean-field model developed by Durif et al. [1] has been presented to assess the impact of different microstructural properties on recrystallized and softening fractions. Several points can be highlighted:

- An higher initial recrystallized fraction lowers the half-softening time.
- An higher initial dislocation density induces higher recrystallization and softening fraction for a given time and temperature.
- To minimize restoration and maximize the plasma facing component lifetime, the initial dislocation density in the deformed grains must be kept low and initial recrystallized fraction must be kept close to zero.
- The impact of initial dislocation density on recrystallization and softening kinetics is higher with higher temperatures.
- Temperature does not modify the impact of initial recrystallized fraction on softening and recrystallization kinetics.
- The current model is not able to take into account the impact of dislocation density distribution and radius distribution on softening fraction.

Some limits of the mean field model used here deserve to be mentioned. First it does not account for the effect of the grain boundary energy. It is known that grain boundary migration is impacted by both dislocations-based stored energy and the grain boundary energy itself [6]. When recrystallization starts, dislocation density plays the major role. Upon recovery, the competition between grain-boundary energy and dislocations-based stored energy is growing. The proposed model is thus not able to describe the end of the annealing process when recrystallization gives room to grain growth to happen. However this last stage is of weak importance compared to the completion of the recrystallization/recovery mechanisms. The model does not account either of grain nucleation. It is assumed here that nuclei are already in place before annealing and that a second nucleation process would not drastically change the results. However this highly depends on the hot deformation process parameters used to manufacture the tungsten samples. Consequently, the current model is able to assess the impact of initial microstructural properties like the global dislocation density in the intermediate phases of recrystallization and softening kinetics. It opens the path for reverse engineering to help optimizing tungsten microstructure regarding lifetime of the plasma facing components.

Appendix

Temperature (°C)	Initial recrystallized fraction (%)	Initial hardness (Hv)	Half-softening time (s)	Recrystallized fraction after 10000s	Hardness after 10000s
1500	5%	444	1705	22	361
1500	15%	435	1282	30	361
1500	25%	426	925	40	361
1600	5%	444	194	74	359
1600	15%	435	131	81	359
1600	25%	426	91	85	359

Table 2. Results of the simulations done with an annealing temperature of 1500°C or 1600°C using different initial recrystallized fraction

Temperature (°C)	Initial dislocation density (m^{-2})	Initial hardness (Hv)	Half-softening time (s)	Dislocation density after 4000s (m^{-2})	Hardness after 4000s (Hv)	Recrystallized fraction after 4000 s (%)	Dislocation density after 10000s (m^{-2})	Hardness after 10000s (Hv)	Recrystallized fraction after 10000 s (%)
1500	$1.6.10^{13}$	402	1499	$1.15.10^{12}$	369	20	$2.2.10^{10}$	360	20
1500	$4.81.10^{13}$	434	1282	$3.46.10^{12}$	375	29	$6.7.10^{10}$	361	30
1500	$1.44.10^{14}$	490	825	$1.04.10^{13}$	400	55	$2.00.10^{11}$	361	57
1550	$1.6.10^{13}$	402	658	$7.18.10^{10}$	361	27	$2.17.10^{7}$	359	27
1550	$4.81.10^{13}$	434	460	$2.16.10^{11}$	361	50	$6.48.10^{7}$	359	50
1550	$1.44.10^{14}$	490	215	$6.46.10^{11}$	360	88	$1.94.10^{8}$	359	89
1600	$1.6.10^{13}$	402	259	$3.98.10^{8}$	359	44	49	359	44
1600	$4.81.10^{13}$	434	131	$1.2.10^{9}$	359	81	150	359	81
1600	$1.44.10^{14}$	490	45	0	359	100	0	359	100

Table 3. Results of the simulations done with an annealing temperature of 1500°C or 1600°C using different initial dislocation density

Temperature (°C)	Distribution parameters of initial radius distribution							Results	
	μ	Σ	Mean value (μm)	Median (μm)	Standard deviation (μm)	First decile (μm)	Last decile (μm)	Recrystallized fraction after 10000 s (%)	Half-softening time (s)
1500	-0.098	1.138	4.50	2.17	5.90	1.22	10.2	33	1234
1500	-0.098	2.138	4.35	1.58	7.02	1.04	10.9	30	1282
1500	-0.098	3.138	3.32	1.22	5.35	1.01	7.40	33	1234
1500	-1.098	2.138	2.94	5.68	4.87	1.02	5.42	32	1243
1500	0.902	2.138	5.68	2.13	8.12	1.09	15.2	30	1283
1550	-0.098	1.138	4.50	2.17	5.90	1.22	10.2	55	423
1550	-0.098	2.138	4.35	1.58	7.02	1.04	10.9	50	460
1550	-0.098	3.138	3.32	1.22	5.35	1.01	7.40	55	422
1550	-1.098	2.138	2.94	5.68	4.87	1.02	5.42	54	430
1550	0.902	2.138	5.68	2.13	8.12	1.09	15.2	50	460
1600	-0.098	1.138	4.50	2.17	5.90	1.22	10.2	87	115
1600	-0.098	2.138	4.35	1.58	7.02	1.04	10.9	82	131
1600	-0.098	3.138	3.32	1.22	5.35	1.01	7.40	88	114
1600	-1.098	2.138	2.94	5.68	4.87	1.02	5.42	86	118
1600	0.902	2.138	5.68	2.13	8.12	1.09	15.2	82	131

Table 4. Parameters of the log-lognormal distribution used to determine the initial radius of the deformed grains and results associated using an annealing temperature of 1500 °C for the simulations

Temperature (°C)	Distribution parameters of initial dislocation density distribution							Results	
	μ	Σ	Mean value (m^{-2})	Median (m^{-2})	Standard deviation (m^{-2})	First decile (m^{-2})	Last decile (m^{-2})	Recrystallized fraction after 10000 s (%)	Half-softening time (s)
1500	0,1096	0.5	$4.70.10^{13}$	$3.04.10^{13}$	$6.25.10^{13}$	$1.80.10^{13}$	$8.19.10^{13}$	47	742
1500	-0.6645	1.5	$4.85.10^{13}$	$1.57.10^{13}$	$1.01.10^{14}$	$1.07.10^{13}$	$9.13.10^{13}$	37	580
1500	-1.6788	3	$3.74.10^{13}$	$1.11.10^{13}$	$9.85.10^{13}$	$1.00.10^{13}$	$5.60.10^{13}$	31	675
1550	0,1096	0.5	$4.70.10^{13}$	$3.04.10^{13}$	$6.25.10^{13}$	$1.80.10^{13}$	$8.19.10^{13}$	75	201
1550	-0.6645	1.5	$4.85.10^{13}$	$1.57.10^{13}$	$1.01.10^{14}$	$1.07.10^{13}$	$9.13.10^{13}$	56	165
1550	-1.6788	3	$3.74.10^{13}$	$1.11.10^{13}$	$9.85.10^{13}$	$1.00.10^{13}$	$5.60.10^{13}$	47	213
1600	0,1096	0.5	$4.70.10^{13}$	$3.04.10^{13}$	$6.25.10^{13}$	$1.80.10^{13}$	$8.19.10^{13}$	98	80
1600	-0.6645	1.5	$4.85.10^{13}$	$1.57.10^{13}$	$1.01.10^{14}$	$1.07.10^{13}$	$9.13.10^{13}$	85	149
1600	-1.6788	3	$3.74.10^{13}$	$1.11.10^{13}$	$9.85.10^{13}$	$1.00.10^{13}$	$5.60.10^{13}$	77	226

Table 5. Parameters of the log-lognormal distribution used to determine the initial dislocation densities of the deformed grains and results associated using an annealing temperature of 1500 °C for the simulations

III. Acknowledgment

This work has been carried out within the framework of the EUROfusion Consortium, funded by the European Union via the Euratom Research and Training Programme (Grant Agreement No 101052200 — EUROfusion). Views and opinions expressed are however those of the author(s) only and do not necessarily reflect those of the European Union or the European Commission. Neither the European Union nor the European Commission can be held responsible for them.

IV. References

[1] A. Durif *et al.*, « Competition between recovery and recrystallization in two tungsten supplies according to ITER specifications », *J Mater Sci*, vol. 57, nº 15, p. 7729-7746, avr. 2022, doi: 10.1007/s10853-022-07123-w.

[2] H. Bolt *et al.*, « Plasma facing and high heat flux materials – needs for ITER and beyond », *Journal of Nuclear Materials*, vol. 307-311, p. 43-52, déc. 2002, doi: 10.1016/S0022-3115(02)01175-3.

[3] R. A. Pitts *et al.*, « Physics basis for the first ITER tungsten divertor », *Nuclear Materials and Energy*, vol. 20, p. 100696, août 2019, doi: 10.1016/j.nme.2019.100696.

[4] T. Hirai *et al.*, « Use of tungsten material for the ITER divertor », *Nuclear Materials and Energy*, vol. 9, p. 616-622, déc. 2016, doi: 10.1016/j.nme.2016.07.003.

[5] A. Durif, M. Richou, G. Kermouche, M. Lenci, et J.-M. Bergheau, « Impact of tungsten recrystallization on ITER-like components for lifetime estimation », *Fusion Engineering and Design*, vol. 138, p. 247-253, 2019, doi: 10.1016/j.fusengdes.2018.11.003.

[6] F. J. Humphreys et M. Hatherly, « Introduction », in *Recrystallization and Related Annealing Phenomena (Second Edition)*, F. J. Humphreys et M. Hatherly, Éd. Oxford: Elsevier, 2004, p. 1-10. doi: 10.1016/B978-008044164-1/50005-0.

[7] F. J. Humphreys et M. Hatherly, « Chapter 7 - Recrystallization of Single-Phase Alloys », in *Recrystallization and Related Annealing Phenomena (Second Edition)*, F. J. Humphreys et M. Hatherly, Éd. Oxford: Elsevier, 2004, p. 215-IV. doi: 10.1016/B978-008044164-1/50011-6.

[8] M. Avrami, « Kinetics of Phase Change. II Transformation-Time Relations for Random Distribution of Nuclei », *The Journal of Chemical Physics*, vol. 8, nº 2, p. 212, déc. 2004, doi: 10.1063/1.1750631.

[9] Johnson et Mehl, « Reaction Kinetics in Processes of Nucleation and Growth », p. 416-442., 1939.

[10] A. Alfonso, D. Juul Jensen, G.-N. Luo, et W. Pantleon, « Recrystallization kinetics of warm-rolled tungsten in the temperature range 1150–1350°C », *Journal of Nuclear Materials*, vol. 455, nº 1, p. 591-594, déc. 2014, doi: 10.1016/j.jnucmat.2014.08.037.

[11] A. Alfonso, D. Juul Jensen, G.-N. Luo, et W. Pantleon, « Thermal stability of a highly-deformed warm-rolled tungsten plate in the temperature range 1100–1250°C », *Fusion Engineering and Design*, vol. 98-99, p. 1924-1928, oct. 2015, doi: 10.1016/j.fusengdes.2015.05.043.

[12] M. Richou *et al.*, « Recrystallization at high temperature of two tungsten materials complying with the ITER specifications », *Journal of Nuclear Materials*, vol. 542, p. 152418, déc. 2020, doi: 10.1016/j.jnucmat.2020.152418.

[13] V. Shah *et al.*, « Recrystallization behaviour of high-flux hydrogen plasma exposed tungsten », *Journal of Nuclear Materials*, vol. 545, p. 152748, mars 2021, doi: 10.1016/j.jnucmat.2020.152748.

[14] Y. Li *et al.*, « Recrystallization-mediated crack initiation in tungsten under simultaneous high-flux hydrogen plasma loads and high-cycle transient heating », *Nucl. Fusion*, vol. 61, nº 4, p. 046018, mars 2021, doi: 10.1088/1741-4326/abe312.

[15] M. Yu *et al.*, « Hardness loss and microstructure evolution of 90% hot-rolled pure tungsten at 1200–1350°C », *Fusion Engineering and Design*, vol. 125, p. 531-536, déc. 2017, doi: 10.1016/j.fusengdes.2017.05.072.

[16] K. Wang *et al.*, « Effects of thickness reduction on recrystallization process of warm-rolled pure tungsten plates at 1350 °C », *Fusion Engineering and Design*, vol. 125, p. 521-525, déc. 2017, doi: 10.1016/j.fusengdes.2017.03.140.

[17] L. Maire, J. Fausty, M. Bernacki, N. Bozzolo, P. De Micheli, et C. Moussa, « A new topological approach for the mean field modeling of dynamic recrystallization », *Materials & Design*, vol. 146, p. 194-207, mai 2018, doi: 10.1016/j.matdes.2018.03.011.

[18] A. Mannheim, J. A. W. van Dommelen, et M. G. D. Geers, « Modelling recrystallization and grain growth of tungsten induced by neutron displacement defects », *Mechanics of Materials*, vol. 123, p. 43-58, août 2018, doi: 10.1016/j.mechmat.2018.04.008.

[19] A. Mannheim, J. A. W. van Dommelen, et M. G. D. Geers, « Controlled irradiation hardening of tungsten by cyclic recrystallization », *Modelling Simul. Mater. Sci. Eng.*, vol. 27, nº 6, p. 065001, mai 2019, doi: 10.1088/1361-651X/ab1eec.

[20] G. Pintsuk, I. Bobin-Vastra, S. Constans, P. Gavila, M. Rödig, et B. Riccardi, « Qualification and post-mortem characterization of tungsten mock-ups exposed to cyclic high heat flux loading », *Fusion Engineering and Design*, vol. 88, nº 9, p. 1858-1861, oct. 2013, doi: 10.1016/j.fusengdes.2013.05.091.

[21] M. Li et J.-H. You, « Interpretation of the deep cracking phenomenon of tungsten monoblock targets observed in high-heat-flux fatigue tests at 20MW/m2 », *Fusion Engineering and Design*, vol. 101, p. 1-8, déc. 2015, doi: 10.1016/j.fusengdes.2015.09.008.

[22] D. Piot *et al.*, « A semitopological mean-field model of discontinuous dynamic recrystallization: Toward a correct and rapid prediction of grain-size distribution », *Journal of Materials Science*, vol. 53, juin 2018, doi: 10.1007/s10853-018-2137-3.

[23] M. Hillert, « On the theory of normal and abnormal grain growth », *Acta Metallurgica*, vol. 13, nº 3, p. 227-238, mars 1965, doi: 10.1016/0001-6160(65)90200-2.

[24] M. Zouari, N. Bozzolo, et R. E. Loge, « Mean field modelling of dynamic and post-dynamic recrystallization during hot deformation of Inconel 718 in the absence of δ phase particles », *Materials Science and Engineering: A*, vol. 655, p. 408-424, févr. 2016, doi: 10.1016/j.msea.2015.12.102.

[25] O. Beltran, K. Huang, et R. E. Logé, « A mean field model of dynamic and post-dynamic recrystallization predicting kinetics, grain size and flow stress », *Computational Materials Science*, vol. 102, p. 293-303, mai 2015, doi: 10.1016/j.commatsci.2015.02.043.

[26] K. Tsuchida, T. Miyazawa, A. Hasegawa, S. Nogami, et M. Fukuda, « Recrystallization behavior of hot-rolled pure tungsten and its alloy plates during high-temperature annealing », *Nuclear Materials and Energy*, vol. 15, p. 158-163, mai 2018, doi: 10.1016/j.nme.2018.04.004.

[27] C. Ren, Z. Z. Fang, L. Xu, J. P. Ligda, J. D. Paramore, et B. G. Butler, « An investigation of the microstructure and ductility of annealed cold-rolled tungsten », *Acta Materialia*, vol. 162, p. 202-213, janv. 2019, doi: 10.1016/j.actamat.2018.10.002.